

# CORE MASS FUNCTION: THE ROLE OF GRAVITY

Sami Dib<sup>1,2</sup>, Axel Brandenburg<sup>3</sup>, Jongsoo Kim<sup>4</sup>, Maheswar Gopinathan<sup>4,5</sup>, and Philippe André<sup>2</sup>

## ABSTRACT

We analyse the mass distribution of cores formed in an isothermal, magnetized, turbulent, and self-gravitating nearly critical molecular cloud model. Cores are identified at two density threshold levels. Our main results are that, in the presence of self-gravity, the slopes of the core mass function (CMF) at the high mass end, in agreement with observations, are shallower than those predicted by the theory of turbulent fragmentation. The shallowness of the slope is due to the effects of core coalescence and gas accretion. Secondly, the slope of the CMF at the high mass end steepens when cores are selected at higher density thresholds. Alternatively, if the CMFs are fitted with a log-normal function, the width of the log-normal distribution decreases with increasing threshold. This is due to the fact that gravity plays a more important role in denser structures selected at higher density threshold and leads to the conclusion that the role of gravity is essential in generating a CMF that bears more resemblance with the IMF when cores are selected with an increasing density threshold in the observations.

*Subject headings:* ISM : clouds – ISM : globules – ISM : kinematics and dynamics – ISM : magnetic fields – turbulence – MHD

## 1. INTRODUCTION

It is now widely accepted that stars form in dense and gravitationally bound molecular cloud (MC) cores. Thus, understanding the properties of the core mass function (CMF) is

---

<sup>1</sup>Lebanese University, Faculty of Sciences, Department of Physics, El Hadath, Beirut, Lebanon; sami.dib@gmail.com

<sup>2</sup>Service d'Astrophysique, CEA/DSM/DAPNIA/SAP, C.E. Saclay, 91191, Gif-sur-Yvette Cedex, France

<sup>3</sup>NORDITA, Roslagstullsbacken 23, AlbaNova University Center, 10691 Stockholm, Sweden

<sup>4</sup>Korea Astronomy and Space Science Institute, 61-1, Hwaam-dong, Yuseong-gu, Daejeon 305-348, Korea

<sup>5</sup>Aryabhata Research Institute of Observational Sciences, Manora Peak, Nainital 263129, India

the cornerstone of any successful theory of the origins of the initial stellar mass function (IMF). The important question whether there is a one-to-one mapping between the CMF and the IMF remains an open one. The CMF is usually represented by  $dN/dM = M^\alpha$  (or  $dN/d(\log M) = M^\Gamma$ , with  $\Gamma = \alpha - 1$ ), where  $\alpha$  takes different values in different mass ranges (for the IMF,  $\alpha = -2.35$  for  $M \gtrsim 0.5 M_\odot$ , Salpeter 1955). In the past few years, the determination of the mass spectra of clumps and cores of several MC regions have been obtained using a variety of wavelengths and techniques such as millimeter spectroscopy of various molecular lines, continuum mm/submm emission from dust, and stellar near infrared absorption by dust. Usually, no prior assumptions are made on the type of structures identified in these studies. They can be a mixture of protostellar envelopes, pre-stellar cores, or unbound objects.

For nearby MCs, where it is possible to identify dense and small (size  $R \lesssim 0.1$  pc) cores, the CMF is usually described by a two component power law above and below a turnover point (with exponents  $\alpha_h$  and  $\alpha_l$ , respectively). In submm/mm observations,  $\alpha_h$  and  $\alpha_l$  are found to be in the range  $[-2.1,-3]$  and  $[-1.3,-1.5]$ , respectively (Motte et al. 1998,2001; Testi & Sargent 2001; Johnstone et al. 2000,2001,2006; Beuther & Schilke 2004; Stanke et al. 2006; Reid & Wilson 2006a,b; Johnstone & Bally 2006; Kirk et al. 2006; Enoch et al. 2006; Young et al. 2006). These estimates bracket the values of the exponents of the IMF (Scalo 1998; Kroupa 2002; Chabrier 2003). Similar IMF-like slopes are found using high density molecular tracers such as  $\text{H}^{13}\text{CO}^+$  (Onishi et al. 2002; Ikeda et al. 2007) and the near infrared absorption technique (Alves et al. 2007). We call these objects IMF like cores (IMFC). On the other hand, submm/mm observations of more distant clouds in which it is only possible to identify larger structures (i.e.,  $R \gtrsim 0.1$  pc), exhibit values of  $\alpha_h$  that are in the range of  $[-1.4,-1.8]$  if the whole mass spectrum is fitted with a single power law (e.g., Coppin et al. 2000; Kerton et al. 2001; Tothill et al. 2002; Mookerjea et al. 2004; Massi et al. 2007; Li et al. 2007, Muñoz et al. 2007) or slightly steeper ( $\alpha_h \sim -2$ ) if it can be fitted by a two component power law (e.g., Reid & Wislon 2005). Similar slopes are obtained from molecular line observations using low to intermediate density molecular line tracers (e.g., Stutzki & Gütsen 1990; Lada et al. 1991; Blitz 1993; Brand & Wouterloot 1995; Dobashi 1996; Yonekura et al. 1997; Kramer et al. 1998; Heithausen et al. 1998; Kawamura et al. 1998; Wilson et al. 2003). We call these objects non-IMF like cores (NIMFC). Values of  $\alpha_h \sim [-1.6, -1.7]$  resemble the slopes of the stellar cluster mass function (Elmegreen 2000), which hints to the fact that these objects cannot be the direct progenitors of individual stars and must undergo additional fragmentation.

The discrepancy in  $\alpha_h$  between the IMFC and NIMFC populations do not seem to be merely an effect of the spatial resolution and hence of mass resolution. In Motte et al. (1998), the inclusion of the larger size cores in the construction of the mass spectrum changes the

values of  $\alpha_h$  from  $-2.5$  to  $\sim -1.5$ . Another example are the results of Coppin et al. (2000) for Orion A North, a region harboring ongoing massive star formation. Although the mass resolution in this study is  $\sim 0.1 M_\odot$ ,  $\alpha_h$  is  $\sim -1.5$ , much shallower than the IMF slope. An explanation of the origin of the discrepancy would be that different physical processes dominate the evolution of these two populations of cores. The close resemblance between the IMFC mass spectra and the IMF suggests that they are more likely to be gravitationally bound and are the direct progenitors of stars or small stellar systems, whereas the NIMFC cores are more likely to be dominated by turbulence. It is important to mention at this stage that the description of the CMF by power law functions is by no means the unique option. Reid et al. (2006b) argued that a log-normal function is a better fit to the observed CMF in many regions. More recently, Goodwin et al. (2007) showed that the CMF of the submillimeter cores obtained by Nutter & Ward-Thompson (2007) is also well represented by a log-normal distribution.

Several physical processes are believed to play a role in shaping the CMF: gravitational fragmentation (e.g., Zinnecker 1984; Klessen 2001), thermal fragmentation (e.g., Li et al. 2003), supersonic turbulence (e.g., Elmegreen 1993; Padoan & Nordlund 2002 PN02), accretion (e.g., Larson 1992; Bonnell et al. 2001; Bate & Bonnell 2005), cores coalescence (e.g., Murray & Lin 1996; Dib et al. 2007a,2008), feedback (Adams & Fatuzzo 1996), and magnetic fields (Shu et al. 2004). A number of numerical studies of MCs that include one or a few of these physical processes have derived a CMF (e.g., Bonnell et al. 2003; Gammie et al. 2003; Li et al. 2004; Ballesteros-Paredes et al. 2006; Padoan et al. 2007). However, these studies have focused on obtaining CMFs that resemble the stellar IMF. The origin of the differences between the IMFC and NIMFC mass spectra, and the eventual link between them has not been investigated so far. In this study, we identify cores in a high resolution 3D numerical simulation of a magnetized, turbulent, and self-gravitating MC model at different density thresholds. In a previous study (Dib et al. 2007b), we have shown, using a detailed virial analysis that the inner parts of dense structures, identified at higher density thresholds, are more gravitationally bound than the same objects identified at lower thresholds. Thus, constructing the CMF at different thresholds is a direct test of the effects of gravity on the CMF. A striking example of how the density threshold can modify the inferred masses of individual cores is the case of the core L1512. Its derived mass from CO observations was estimated at  $\sim 6 M_\odot$  (Falgarone et al. 2001), whereas it was estimated from submm observations at  $\sim 1.4 M_\odot$  (Ward-Thompson et al. 1999). Another example is the case of the NGC 7538 region, observed by Kramer et al. (1998) to have a mass spectra slope of  $\alpha_h = -1.65$  in the  $^{13}\text{CO}(1-0)$  line and  $\alpha_h = -1.79$  in the  $\text{C}^{18}\text{O}(1-0)$  line which traces higher density material.

## 2. THE SIMULATIONS, CLUMP-FINDING ALGORITHM, AND ANALYSIS STRATEGY

We performed a 3D numerical simulation of a magnetized, self-gravitating, and turbulent isothermal MC using the TVD code (Kim et al. 1999). The simulation is similar to the ones presented in Dib et al. (2007b) but repeated with a higher numerical resolution of  $512^3$  grid cells. In Dib et al. (2007b), we found that the population of cores formed in a moderately magnetically supercritical (i.e.,  $\mu = 2.8$ ) cloud reproduce best some of the available observations such as the virial parameter-mass relation. Thus, we here only consider this cloud model for further analysis. We recall the basic features of this simulation: Turbulence is driven until it is fully developed (i.e., for 2 crossing timescales) before gravity is turned on. The Poisson equation is solved to account for the self-gravity of the gas using a standard Fourier algorithm. Turbulence is constantly driven in the simulation box following the algorithm of Stone et al. (1998). The kinetic energy input rate is adjusted such as to maintain a constant rms sonic Mach number  $M_s = 10$ . Kinetic energy is injected at large scales, in the wave number range  $k = 1 - 2$ . Periodic boundary conditions are used in the three directions. In physical units, the simulation has a linear size of 4 pc, an average number density of  $\bar{n} = 500 \text{ cm}^{-3}$ , a temperature of 11.4 K, a sound speed of  $0.2 \text{ km s}^{-1}$ , and an initial *rms* velocity of  $2 \text{ km s}^{-1}$ . The Jeans number of the box is  $J_{box} = 4$  (i.e., number of Jeans masses in the box is  $M_{box}/M_{Jeans,box} = J_{box}^3 = 64$ , where  $M_{box} = 1887 M_\odot$ ). The initial magnetic field strength in the box for this model is  $B_0 = 14.5 \mu\text{G}$ . Correspondingly, the  $\beta$  plasma and mass-to-magnetic flux (normalized for the critical value for collapse  $M/\phi = 0.12 G^{-1/2}$ , Tomisaka et al. 1988) values of the box are  $\beta_p = 0.1$ , and  $\mu_{box} = 2.8$ .

Cores are identified using a clump-finding algorithm that is based on a density threshold criterion and a friend-of-friend approach and is described in detail in Dib et al. (2007b). We restrict our selection of cores to epochs where the Truelove criterion (Truelove et al. 1997) is not violated in any of them. Thus our derived CMF applies to starless prestellar cores. At a given threshold, the number of cores detected at one epoch is insufficient to sample appropriately the whole mass spectrum. It is therefore necessary to combine cores selected at several epochs in order to construct a mass spectrum that is statistically significant. We combine the populations of cores identified at 35 timesteps. This approach resembles the situation in the observations where cores identified in different locations of a MC are most likely in different stages of their evolution. Even for a composite multi-epoch spectrum, the statistics of cores identified with thresholds above  $\gtrsim 60 \bar{n}$  remains poor.

### 3. CORE MASS FUNCTION

Before discussing the CMF obtained from the simulation, it is worth to check what CMF would be anticipated from the turbulent fragmentation theory of PN02. Fig. 1 displays the time evolution of the exponent of the turbulent velocity field power spectrum,  $\beta$  (top), and a few velocity spectra at selected epochs (bottom). The values of  $\beta$  are observed to fluctuate around the value of 1.9. According to PN02, this would result in a CMF slope at the high mass end of  $\alpha_h \sim -2.42$  (at a given epoch and for a multiple-epoch built CMF). Fig. 2 displays the CMF for populations of cores identified at the density thresholds of 20 and 50  $\bar{n}$ . Both samples use the same number of time-steps, therefore, they are free from any bias in the temporal selection. Several features of the CMFs can be noted. If the high-mass end of the spectra is to be assimilated to a power law, fits to the CMF in the high mass end yield a steeper slope for the high density threshold sample than for the one with the lower threshold. The slopes for the 20  $\bar{n}$  and 50  $\bar{n}$  are  $-1.55 \pm 0.15$  and  $-1.80 \pm 0.2$ , respectively. However, the CMFs are also well fitted over their entire mass range by a log-normal distribution whose width is smaller at higher threshold. The width of the CMF (with logarithmic mass bins) is  $1.63 \pm 0.07$  and  $1.12 \pm 0.09$  at the 20 and 50  $\bar{n}$  levels, respectively (i.e., the width of the IMF is 0.57, Chabrier 2003).

Obviously, the slope of the CMF at high mass end is shallower than what is predicted by PN02 and steepens with increasing threshold. We interpret the shallower than the IMF slopes and the steepening with increasing threshold by the dual effect played by gravity in the presence of turbulence. The steepening of the slope with increasing threshold is due to the increasing importance of gravity at higher thresholds. Fig. 3 displays the ratio of the gravitational term in the virial theorem ( $W = -\int_V \rho r_i (\partial\phi/\partial r_i) dV$ , where  $\phi$  is the gravitational potential) to the other terms that appear in the virial equation. The latter terms are condensed in the quantity  $\Theta_{VT} = 2 (E_{th} + E_k - \tau_k - \tau_{th}) + E_{mag} + \tau_{mag}$ , where  $E_{th} = \frac{3}{2} \int_V P dV$  is the volume thermal energy, with  $P$  being the thermal pressure,  $E_k = \frac{1}{2} \int_V m_i v_i^2 dV$  the volume kinetic energy,  $E_{mag} = \frac{1}{8\pi} \int_V B^2 dV$  the volume magnetic energy,  $\tau_{th} = \frac{1}{2} \oint_S r_i P \hat{n}_i dS$  the surface thermal energy,  $\tau_k = \frac{1}{2} \oint_S r_i \rho v_i v_j \hat{n}_j dS$  the surface kinetic energy, and  $\tau_{mag} = \oint_S r_i T_{ij} \hat{n}_j dS$  the surface magnetic energy, where  $T_{ij}$  is the Maxwell stress tensor. What Fig. 3 indicates is that gravity is more important in the virial balance for the sample of cores defined at the 50  $\bar{n}$  threshold than for the cores defined at the 20  $\bar{n}$  threshold. An extrapolation to higher thresholds of the order of 500  $\bar{n} = 2.5 \cdot 10^5 \text{ cm}^{-3}$  which are number densities similar to those of gravitationally bound cores observed in the submm/mm and in dense molecular tracers such as the  $\text{NH}_3$  and  $\text{HCO}^+$  would yield slopes in the range [-2.3,-2.5], thus offering a natural explanation for the observed slopes of the IMFC cores and the origin of the IMF.

The question rises why is the slope of these CMFs shallower than the slope of the IMF especially for the CMF of the  $20 \bar{n}$  cores that whose structures are more dominated by turbulence and thus should be more adequately described by the PN02 theory. The reason of the discrepancy lies in the fact that in the presence of gravity, the CMF is non-stationary as implied by PN02. Fig. 4 displays the time evolution, for the  $20 \bar{n}$  cores, of the fraction of the mass present in the cores, number of cores, average mass of the cores, and median mass of the cores. The increasing mass fraction and average mass of the cores and the constancy of the number of cores and their median mass are a clear indication of mass growth affecting the cores due to the combined effect of gas accretion and core coalescence (for an example of core coalescence in our simulations see Figure 16 in Dib et al. 2007b). Although it is not possible to assess from Fig. 4 the contribution of each of these two processes, this mass growth which constitutes a deviation to the PN02 theory is responsible for shallower slopes than expected by this theory.

#### 4. CONCLUSIONS

In this work, we have constructed the mass function of cores in a 3D numerical simulation of a magnetized, turbulent, and self-gravitating molecular cloud (MC). Cores are identified at the density threshold levels of  $10^4$  and  $2.5 \times 10^4 \text{ cm}^{-3}$ . In agreement with observations, the slope of the core mass function (CMF) is found to be steeper for cores identified at the higher threshold level. The steepening of the slope with increasing threshold is due to the increasing importance of gravity in the virial balance of the cores when they are identified at higher thresholds and a sign of the role played by turbulence assisted gravitational fragmentation (i.e., gravo-turbulent fragmentation). On the other hand, these slopes are shallower than what is predicted by the theory of pure turbulent fragmentation (Padoan & Nordlund 2002). This can be explained by the effects of mass growth observed to affect the cores in the presence of gravity. This mass growth is essentially due in the initial phase to the effect of core coalescence which generates more massive structures particularly for cores defined at lower thresholds since they have larger cross sections. Although turbulence is an essential ingredient that will generate an initial distribution of core masses in an initial homogeneous medium, our results suggest that, in a self-gravitating cloud, it is the effects of self-gravity coupled to turbulence rather than pure turbulent fragmentation that sets the slope of the CMF that can be measured for cores identified at a given density threshold and that is ultimately responsible for the generation of a CMF that resembles the initial stellar mass function.

S.D. and A.B. acknowledge the hospitality of the Kavli Institute for Theoretical Physics

at the University of California Santa Barbara which enabled their participation in the Star Formation Through Cosmic Time program through NSF grant No PHY05-51164. Simulations were performed on a high performance cluster that was built with funding from the Korea Astronomy and Space Science Institute and the Astrophysical Research Center for the Structure and Evolution of the Cosmos (ARCSEC) of the Korea Science and Engineering Foundation (KOSEF). J.K. was supported in part by KOSEF through ARCSEC and the grant of the basic research program R01-2007-000-20196-0.

## REFERENCES

- Adams, F. C., & Fatuzzo, M. 1996, *ApJ*, 464, 256
- Alves, J., Lombardi, M., & Lada, C. J. 2007, *A&A*, 462, L17
- Ballesteros-Paredes, J., Gazol, A., Kim, J., Klessen, R. S., Jappsen, A.K., & Tejero, E. 2006, *ApJ*, 637, 384
- Bate, M. R., & Bonnell, I. A. 2005, *MNRAS*, 356, 1201
- Beuther, H., & Schilke, P. 2004, *Science*, 303, 1167
- Blitz, L. 1993, in *Protostars and Planets III*, ed. E. H. Levy & J. I. Lunine (Tucson:Univ. Arizona Press), 125
- Bonnell, I., Clarke, C. J., Bate, M. R., & Pringle, J. E. 2001, *MNRAS*, 324, 573
- Bonnell, I., Bate, M. R., & Vine, S. G. 2003, *MNRAS*, 343, 413
- Brand, J., Wouterloot, J. G. A. 1995, *MNRAS*, 303, 851
- Chabrier, G. 2003, *PASP*, 115, 763
- Coppin, K. E. K., Greaves, J. S., Jenness, T., & Holland, W. S. 2000, *ApJ*, 356, 1031
- Dib, S., Kim, J., Vázquez-Semadeni, E., Burkert, A., & Shadmehri, M. 2007a, *ApJ*, 661, 262
- Dib, S., Kim, J., Shadmehri, M. 2007b, *MNRAS*, 381, L40
- Dib, S., Shadmehri, M., Maheswar, G., Kim, J., & Henning, T. 2008, in the proceedings of the meeting "Massive Star Formation: Observations confront Theory". ASP Conf. Series, (arXiv:0710.3969)
- Dobashi, K., Bernard, J. P., & Fukui, Y. 1996, *ApJ*, 466, 282

- Elmegreen, B. G. 1993, *ApJ*, 419, L29
- Elmegreen, B. G., Efremov, Y. N., Pudritz, R. E., & Zinnecker, H. 2000, in *Protostars and Planets IV*, ed. V. Mannings, A. P. Boss, & S. S. Russel (Tuscon:Univ. Arizona Press), 179
- Enoch, M. L., Young, K. E., Glenn, J. et al. 2006, *ApJ*, 638, 293
- Falgarone, E., Pety, J., & Phillips, T. G. 2001, 555, 178
- Gammie, C. F., Lin, Y.-T., Stone, J., M., & Ostriker, E. C. 2003, *ApJ*, 592, 203
- Goodwin, S. P., Nutter, D., Kroupa, P., Ward-Thompson, D., Whitworth, A. P. *A&A*, in press, (arXiv:0711.1749)
- Heithausen, A., Bensch, F., Stutzki, J., Falgarone, & E. Panis, J.-F. 1998, *A&A*, 331, L65
- Ikeda, N., Sunada, K., & Kitamura, Y. 2007, *ApJ*, 665, 1194
- Johnstone, D., Wilson, C. D., Moriarty-Schieven, G., Joncas, G., Smith, G., Gregersen, E., & Fich, M. 2000, *ApJ*, 545, 327
- Johnstone, D., Fich, M., Mitchell, G. F., & Moriarty-Schieven, G. 2001, *ApJ*, 559, 307
- Johnstone, D., Matthews, H., & Mitchell, G. F. 2006, *ApJ*, 639, 259
- Johnstone, D., & Bally, J. 2006, *ApJ*, 653, 383
- Kawamura, A., Onishi, T., Yonekura, Y., Dobashi, K., Mizuno, A., Ogawa, H., & Fukui, Y. 1998, *ApJS*, 117, 387
- Kerton, C. R., Martin, P. G., Johnstone, D., & Ballantyne, D. R. 2001, *ApJ*, 552, 601
- Kim, J., Ryu, D., Jones, T. W., & Hong, S. S. 1999, *ApJ*, 514, 506
- Kirk, H., Johnstone, D., & Di Francesco, J. 2006, *ApJ*, 1009, 1023
- Klessen, R. S. 2001, *ApJ*, 556, 837
- Kramer, C., Stutzki, J., Rörig, R., & Corneliussen, U. 1998, *A&A*, 329, 249
- Kroupa, P. 2002, *Science*, 295, 82
- Lada, E. A., Bally, J., & Stark, A. A. 1991, *ApJ*, 368, 432
- Larson, R. B. 1992, *MNRAS*, 256, 641

- Li, D., Velusamy, T., Goldsmith, P. F., & Langer, W. D. 2007, *ApJ*, 655, 351
- Li, P. S., Norman, M. L., Mac Low, M.-M., & Heitsch, F. 2004, *ApJ*, 605, 800
- Li, Y., Klessen, R. S., Mac Low, M.-M. 2003, *ApJ*, 592, 975
- Massi, F., De Luca, M., Elia, D., Giannini, T., Lorenzetti, D., Nisini, B. 2007, *A&A*, 466, 1013
- Mookerjea, B., Kramer, C., Nielbock, M., & Nyman, L.-Å 2004, *A&A*, 426, 119
- Motte, F., André, P., Neri, R. 1998, *A&A*, 336, 150
- Motte, F., André, P., Ward-Thompson, D., & Bontemps, S. 2001, *A&A*, 372, L41
- Murray, S. D., & Lin, D. N. C. 1996, *ApJ*, 467, 728
- Muñoz, D. J., Mardone, D., Garay, G., Rebolledo, D., Brooks, K., & Bontemps, S. 2007, *ApJ*, 668, 906
- Onishi, T., Mizuno, A., Kawamura, A., Tachihara, K., & Fukui, Y. 2002, *ApJ*, 575, 950
- Padoan, P., & Nordlund, Å. 2002, *ApJ*, 576, 870
- Padoan, P., Nordlund, Å., Kritsuk, A., Norman, M. L., & Li, P.-S. 2007, *ApJ*, 661, 972
- Reid, M. A., Wilson, C. D. 2005, *ApJ*, 625, 891
- Reid, M. A., & Wilson, C. D. 2006a, *ApJ*, 644, 990
- Reid, M. A., & Wilson, C. D. 2006b, *ApJ*, 650, 970
- Salpeter, E. E. 1955, *ApJ*, 121, 161
- Scalo, J., *The Stellar Initial Mass Function*, Eds. G. Gilmore & D. Howell, 1998, *ASP Conf. Ser.*, 142, 201
- Shu, F. H., Li, Z.-Y., & Allen, A. 2004, *ApJ*, 601, 930
- Stanke, T., Smith, M. D., Gredel, R., & Khanzadyan, T. 2006, *A&A*, 447, 609
- Stone, J. M., Ostriker, E. C., & Gammie, C. F. 1998, *ApJ*, 508, L99
- Stutzki, J., & Gütsen, R. 1990, *ApJ*, 356, 513
- Testi, L., & Sargent, A. I. 1998, *ApJ*, 508, L91

- Tomisaka, K., Ikeuchi, S., & Nakamura, T. 1988, 335, 239
- Tothill, N. F. H., White, G. J., Matthews, H. E. McCutcheon, W. H., McCaughrean, M. J., Kenworthy, M. A. 2002, ApJ, 580, 285
- Truelove, J. K., Klein, R. I., McKee, C. F., Holliman II, J. H., structures H., & Greenough, J. A. 1997, ApJ, 489, L179
- Ward-Thompson, D., Motte, F., André, P. 1999, MNRAS, 305, 143
- Wislon, C. D., Scoville, N., Madden, & S. C. Charmandaris, V. 2003, ApJ, 599, 104
- Yonekura, Y., Dobashi, K., Mizuno, A., Ogawa, H., & Fukui, Y. 1997, ApJS, 110, 21
- Young, K., Enoch, M. L. Evans II, N. J. et astationary ApJ, 644, 326
- Zinnecker, H. 1984, MNRAS, 210, 43

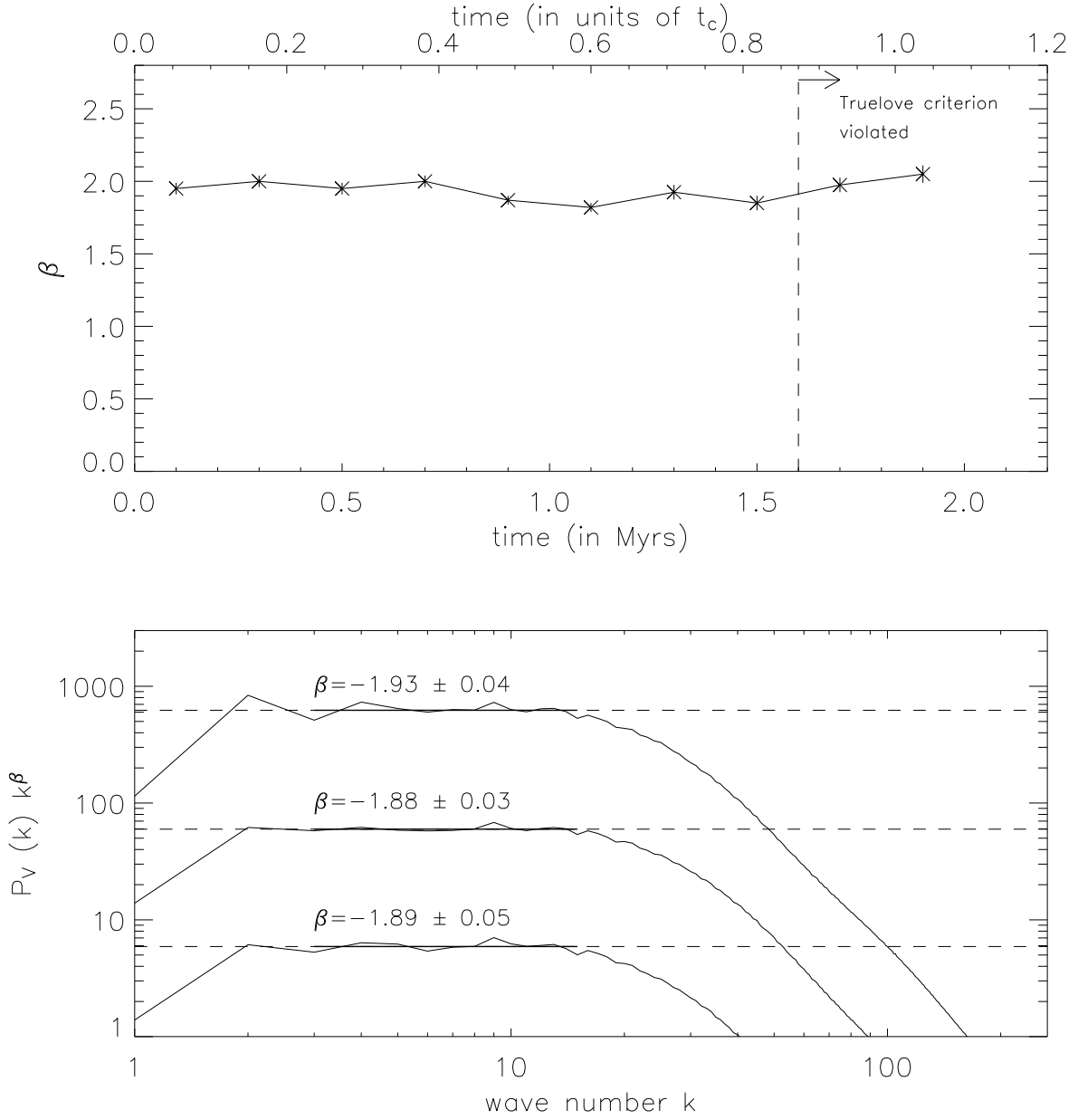


Fig. 1.— Time evolution of the exponent of the turbulent velocity field power spectrum,  $\beta$  (top) and a sample of velocity power spectra at selected epochs (bottom). Each data point in the top figure is an average over five neighboring timesteps.

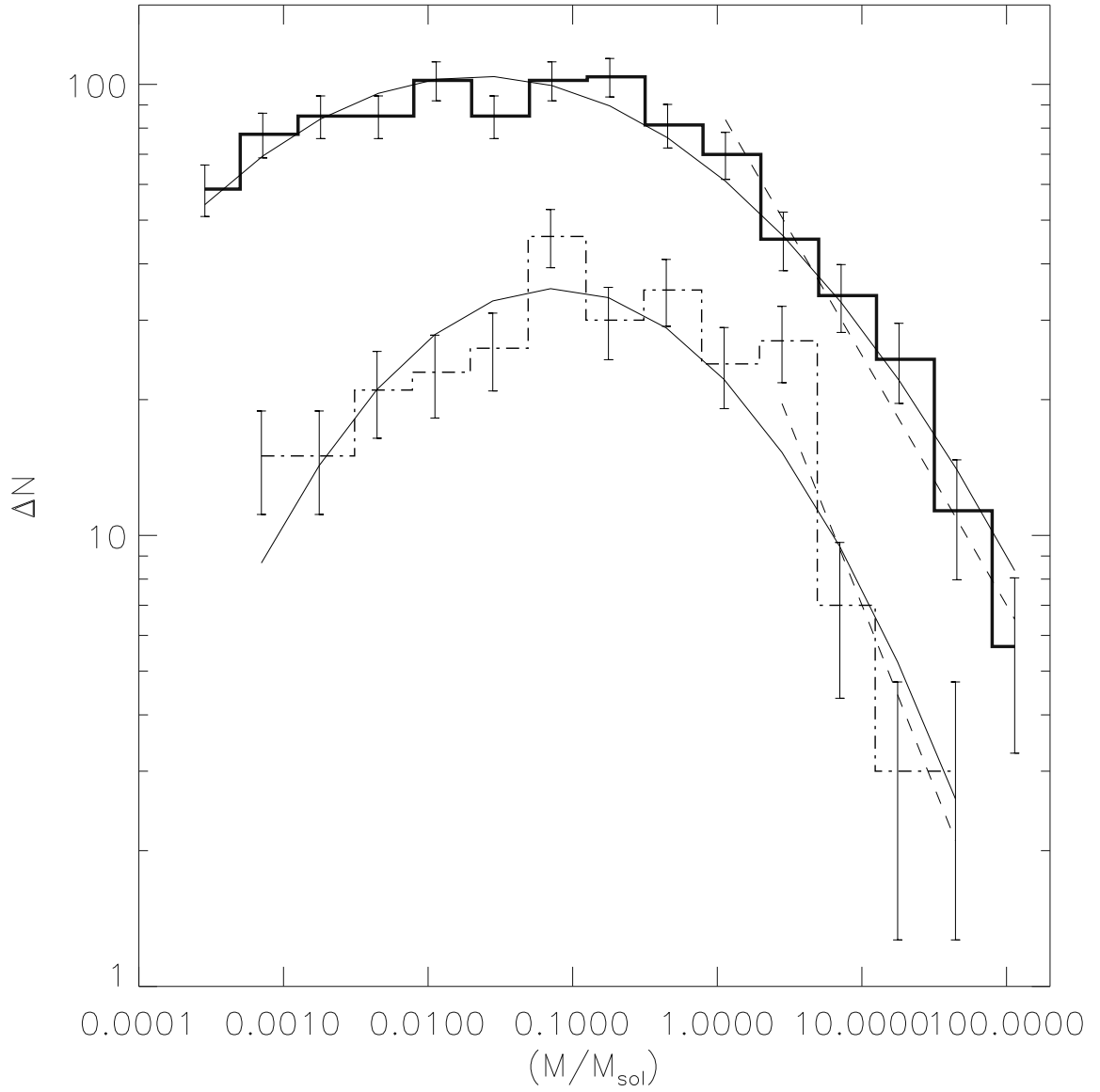


Fig. 2.— The mass function of cores identified in the simulation at the thresholds of  $n_{\text{thr}} = 20 \bar{n}$  (thick line) and  $50 \bar{n}$  (thin dash-dotted line). Overplotted to the results are log-normal fits (thin line) and power law fits to the high mass end of the spectra (dashed line).

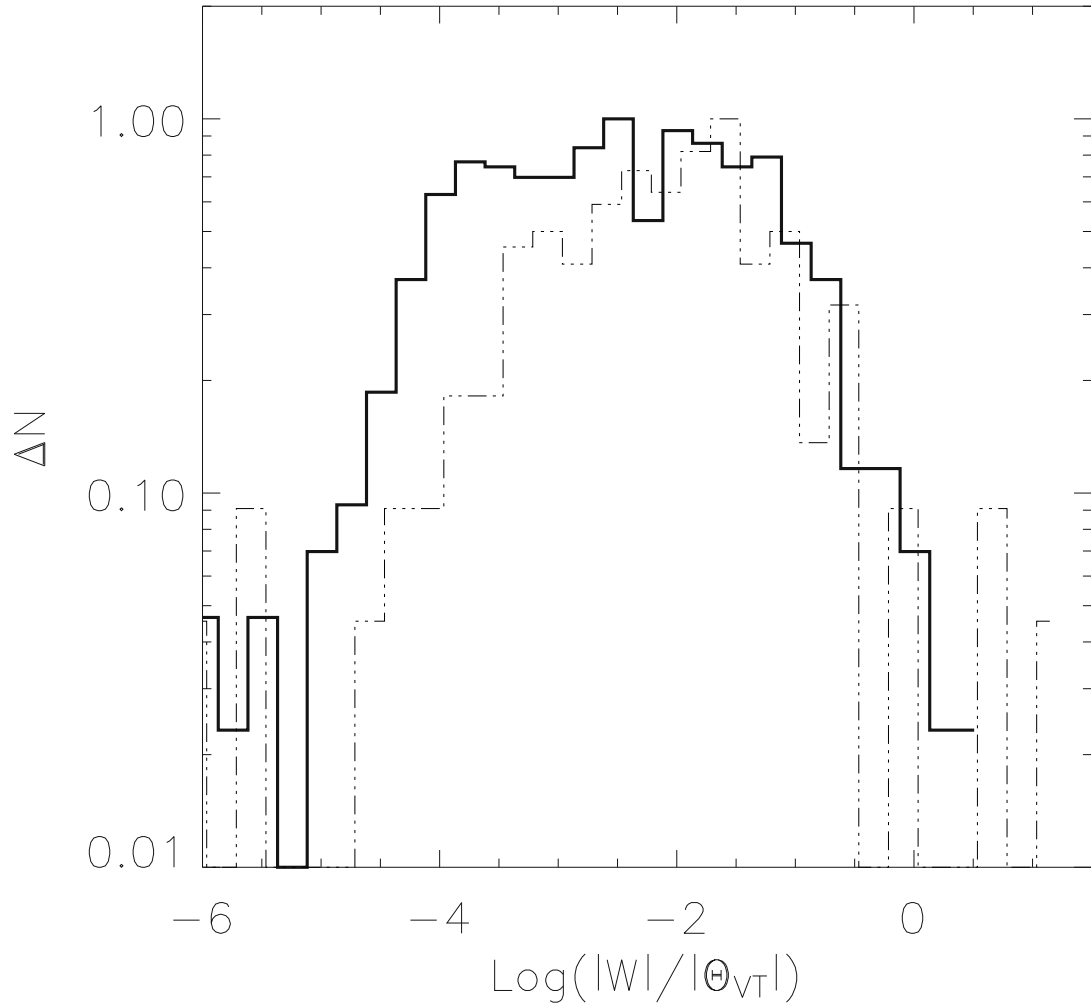


Fig. 3.— Probability distribution function of the ratio of the gravitational term  $W$  to the other, both volume and surface, energy terms that appear in the virial equation (kinetic, thermal, and magnetic). The latter terms are condensed in the quantity  $\Theta_{VT}$  (details are given in the text). The larger the ratio  $|W|/|\Theta_{VT}|$ , the stronger the influence of gravity is.

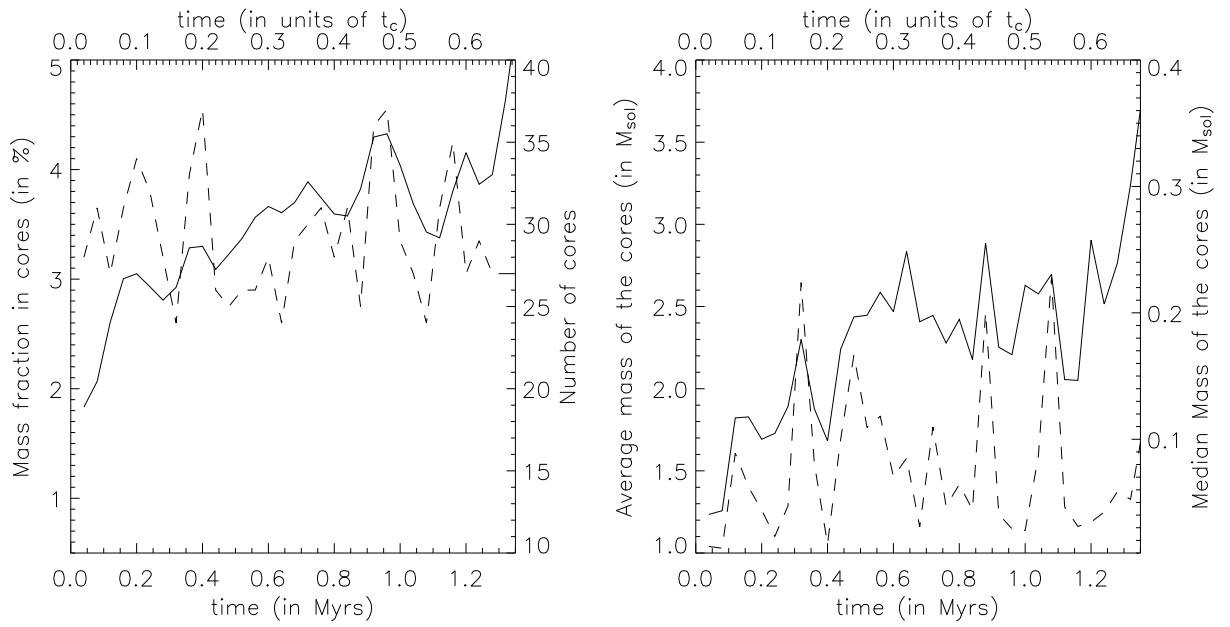


Fig. 4.— Time evolution of: The fraction of the mass present in the cores (left, full line), number of cores (left, dashed line), average mass of the cores (right, full line), and median mass of the cores (left, dashed line). Time is shown in Myrs (bottom) and in units of the crossing time (top).